

1 **THERMAL CONDUCTIVITY FUNCTION FOR FINE-GRAINED UNSATURATED SOILS**
2 **LINKED WITH WATER RETENTION BY CAPILLARITY AND ADSORPTION**

3 **By Y. Lu, Ph.D.¹ and J.S. McCartney, Ph.D., P.E., F.ASCE²**

4 **ABSTRACT**

5 A thermal conductivity function (TCF) is proposed for unsaturated fine-grained soils
6 describing the evolution in thermal conductivity with degree of saturation at room temperature and
7 having parameters associated with the different mechanisms of water retention. Calibration with
8 data from different fine-grained soils reveals that the proposed TCF captures the sigmoidal
9 evolution in thermal conductivity with degree of saturation with a better fit to data in the low and
10 high saturation regimes compared to other TCFs. Correlations between the parameters of the
11 proposed TCF with those of a soil-water retention curve (SWRC) that considers both capillarity
12 and adsorption water retention mechanisms confirm the coupling between these thermo-hydraulic
13 relationships. Thermal conductivity values at degrees of saturation of 1 and 0 can be obtained from
14 experiments on saturated and dry specimens, and the parameters of the new thermal conductivity
15 function correlate linearly with the degree of saturation at maximum adsorption and the SWRC
16 pore size distribution parameter. A strong correlation was also observed between the maximum
17 suction and thermal conductivity in dry conditions, possibly due to effects of mineralogy and dry
18 density on these parameters. A successful validation example for compacted bentonite indicates
19 that consideration of the mechanisms of water retention permits deeper insight into linkages
20 between the TCF and SWRC for fine-grained soils.

¹Postdoctoral Researcher, Department of Structural Engineering, University of California San Diego, 9500 Gilman Dr., La Jolla, CA 92093-0085; Email: yul204@ucsd.edu

²Professor, Department of Structural Engineering, University of California San Diego, La Jolla, CA 92093-0085; Email: mccartney@ucsd.edu

21 INTRODUCTION

22 The thermal conductivity of a given soil at a constant density is a function of the degree of
23 saturation, with a minimum thermal conductivity in dry conditions and a maximum thermal
24 conductivity in saturated conditions, and the thermal conductivity increases with dry density (e.g.,
25 [Johansen 1975](#); [McCartney et al. 2013](#); [Yao et al. 2019](#)). Numerical simulations of coupled heat
26 transfer and water flow in unsaturated soils require a functional relationship between thermal
27 conductivity and the degree of saturation, referred to as the thermal conductivity function (TCF).
28 For example, the TCF plays a major role in heat transfer analyses for unsaturated bentonite buffers
29 in nuclear waste repositories ([Zheng et al. 2010](#)) and energy piles in unsaturated soils ([Behbehani](#)
30 [and McCartney 2022](#)).

31 Empirical TCFs with a single fitting parameter have been proposed by Johansen ([1975](#)), Côté
32 and Konrad ([2005](#)), and Lu et al. ([2007](#)). While simple, the single fitting parameter limits the
33 degree of nonlinearity needed to match experimental thermal conductivity data. Dong et al. ([2015](#))
34 hypothesized that the TCF and SWRC were linked with different trends in thermal conductivity in
35 each of the water retention regimes (i.e., capillary, funicular, pendular). The SWRC describes the
36 relationship between the degree of saturation S and matric suction ψ in soils, which is intrinsically
37 related to the pore size distribution of the soil and indirectly reflects the connectivity between
38 particles which affects conductive heat transfer ([Likos 2014](#)). Lu and Dong ([2015](#)) proposed a TCF
39 whose parameters could be linked to the shape of the SWRC, as follows:

$$\frac{\lambda - \lambda_{\text{dry}}}{\lambda_{\text{sat}} - \lambda_{\text{dry}}} = 1 - \left[1 + \left(\frac{S}{S_f} \right)^\gamma \right]^{1/\gamma-1} \quad (1)$$

40 where λ is the thermal conductivity, λ_{dry} and λ_{sat} are the thermal conductivity at dry and fully
41 saturated conditions, respectively, S_f is the degree of saturation from the SWRC at the onset of the
42 funicular water retention regime which has a linear relationship with the residual saturation S_{res} ,

43 and γ is the pore fluid network connectivity parameter linked to the pore size distribution parameter
 44 n in the van Genuchten (1980) SWRC. The TCF of Lu and Dong (2015) has a more nonlinear
 45 shape than previous TCFs, and its parameters were found to have a strong correlation with the van
 46 Genuchten (1980) SWRC for a range of soil types. However, a notable issue with the form of their
 47 TCF is that it does not converge to λ_{sat} when $S = 1$. Accordingly, the value of λ_{sat} in Eq. (1) must
 48 be treated as a fitting parameter that is larger than the experimentally-measured value of λ_{sat} for a
 49 saturated soil and does not have a physical meaning. This aspect of Eq. (1) may also affect the
 50 quality of correlations between the parameters of the TCF and those of the SWRC. Another issue
 51 is that the SWRC of many fine-grained soils, in particular high plasticity clays, are better
 52 represented by the SWRC of Lu (2016) which considers water retention by capillarity and
 53 adsorption mechanisms, as follows:

$$\begin{aligned}
 S(\psi) &= \frac{1}{\theta_s} [\theta_a(\psi) + \theta_c(\psi)] \\
 &= \frac{\theta_{a,\text{max}}}{\theta_s} \left\{ 1 - \left[\exp\left(\frac{\psi - \psi_{\text{max}}}{\psi}\right) \right]^m \right\} \\
 &\quad + \frac{1}{2\theta_s} \left[1 - \operatorname{erf}\left(\sqrt{2} \frac{\psi - \psi_c}{\psi_c}\right) \right] [\theta_s - \theta_a(\psi)] [1 + (\alpha\psi)^n]^{1/n-1}
 \end{aligned} \tag{2}$$

54 where θ_s is the saturated volumetric water content which is equal to the porosity, $\theta_a(\psi)$ is the
 55 adsorptive volumetric water content, $\theta_c(\psi)$ is the capillary volumetric water content, ψ_{max} is the
 56 maximum matric suction, ψ_c is the mean cavitation suction, $\theta(\psi)$ is volumetric water content
 57 corresponding to a given value of matric suction ψ , $\theta_{a,\text{max}}$ is the adsorption capacity representing
 58 the maximum adsorptive volumetric water content, α is a parameter related to the inverse of the
 59 air-entry pressure of the soil, n is a parameter reflecting the pore size distribution of the soil, and
 60 m is a parameter reflecting the SWRC shape in the adsorption regime.

61 NEW THERMAL CONDUCTIVITY MODEL

62 A new isothermal thermal conductivity function for unsaturated soils is proposed:

$$\frac{\lambda - \lambda_{\text{dry}}}{\lambda_{\text{sat}} - \lambda_{\text{dry}}} = \left[1 - \frac{1 - S^\eta}{1 + \left(\frac{S}{S_c}\right)^\eta} \right]^{1-1/\eta} \quad (3)$$

63 where S_c is the degree of saturation at the onset of the capillary water retention regime, and η is a
64 model parameter that reflects the changing rate of the thermal conductivity with the degree of
65 saturation. The latter parameter reflects the pore size distribution and the pore water network
66 connectivity among soil particles and is hypothesized to be related to the pore-size parameter n in
67 the SWRC model of Lu (2016). The two other TCF parameters also have physical meaning: λ_{dry}
68 and λ_{sat} correspond to the minimum and maximum values of thermal conductivity in dry and
69 saturated conditions, respectively. An advantage of Eq. (3) over Eq. (1) is that the value of λ_{sat} can
70 be obtained from a measurement of the thermal conductivity at saturated conditions instead of
71 from model fitting. When $S = 1$, Eq. (3) degenerates to $\lambda = \lambda_{\text{sat}}$; when $S = 0$, Eq. (3) degenerates to
72 $\lambda = \lambda_{\text{dry}}$. While previous studies found that the thermal conductivity is sensitive to applied stress
73 (Cao et al. 2021), void ratio (McCartney et al. 2013; Yao et al. 2019), and variables affecting
74 particle connectivity like gradation, particle shape and cementation (Xiao et al. 2018; 2020; 2021),
75 the proposed SWRC-linked TCF is developed based on constant volume conditions as the
76 parameters, including λ_{dry} , λ_{sat} , S_c , η , are related to the void ratio and pore size distribution. A
77 similar assumption was also adopted by Lu and Dong (2015). While studies like Cao et al. (2021)
78 considered other heat transfer mechanisms to develop a temperature-dependent TCF, the TCF
79 developed in this study focuses only on conduction and is not temperature dependent as other heat
80 transfer mechanisms can be considered explicitly in analyses (e.g., Behbehani and McCartney
81 2022).

82 MODEL CALIBRATION AND COMPARISON WITH OTHER MODELS

83 To calibrate the proposed TCF and to assess its performance in representing experimental data,
84 data from thermal conductivity tests on ten fine-grained soils, ranging from silts to clays, were
85 obtained from the literature. All these soils had water retention curve data available. Soils 1 and 2
86 were grouped as low plasticity soil, and soils 3 and 4 were grouped as high plasticity natural and
87 remolded soils. Six compacted bentonites (soils 5-10) typically used as backfill materials in the
88 buffers for nuclear waste repositories were grouped together. One common feature of these soils
89 is the SWRC pore size distribution parameter n is less than 2, which is common for fine-grained
90 soil that exhibits a monotonic evolution in suction stress with increasing matric suction (Lu et al.
91 2010). The physical, thermal, and hydraulic properties of these soils are listed in Table 1.

92 The fitting results by the TCFs of Côté and Konrad (2005), Lu et al. (2007), and Lu and Dong
93 (2015) are also included in this analysis. In the fitting of the new TCF, the values of λ_{dry} and λ_{sat}
94 measured experimentally (when available) were used directly in the equation and only S_c and η
95 were used as fitting parameters. Note that most of the values of λ_{dry} in Table 1 were measured in
96 the laboratory, while estimates were made based on the fitting for four soils that did not have
97 measured values (soils 5-7, and 9). In the fitting of the TCF of Lu and Dong (2015), the value of
98 λ_{sat} was used as an additional fitting parameter as the experimentally-derived value of λ_{sat} as it was
99 not possible to incorporate the measured value of λ_{sat} into their equation when $S = 1$. The fittings
100 of the proposed TCF to the data for the ten soils are presented in Figs. 1 and 2. The fitting
101 parameters were obtained by least-squares regression, which permitted definition of the coefficient
102 of determination (R^2) and the root mean square error ($RMSE$) for evaluation of the difference
103 between the measured data and predicted values. These values are reported in Table 2 for the fits
104 of the newly proposed TCF and those of the other models. The best fitting of the four models with

105 the highest value of R^2 was marked in bold. In most cases the newly proposed TCF had the best fit
106 to the data, while in the rest of the cases the TCF had the second best fit.

107 For the ten soils in Table 1, the thermal conductivity varied from 0.210 W/mK for dry
108 conditions to 1.556 W/mK for saturated conditions, showing a wide range of thermal conductivity.
109 Although the TCFs of Côté and Konrad (2005) and Lu et al. (2007) show acceptable fits for some
110 soils, the TCF of Lu and Dong (2015) model and the newly proposed TCF have a better fit to the
111 data for most of the soils. Furthermore, compared with the TCF of Lu and Dong (2015), the TCF
112 proposed in this study has a better fit to the data for most soils. This better fit was achieved with
113 one fewer fitting parameter in the new TCF as the value of λ_{sat} in the new model was fixed to the
114 experimentally-measured value (when available). An inconsistency between the fitted Lu and
115 Dong (2015) TCF and measured data is observed in the high saturation range due to the form of
116 their equation when S approaches 1 which is not present in the fitted proposed TCF.

117 The shape of the TCFs and the model parameters correspond with the soil texture. For instance,
118 a more significant sigmoidal development with a flat shape at low degrees of saturation is exhibited
119 for higher plasticity clay soils. The thermal conductivity is relatively insensitive in the hydration
120 water retention regime because the increase of saturation typically preferentially occurs in the
121 micro-pores within the clay particles (Dong et al. 2015; Lu et al. 2021). Additionally, the TCF
122 parameter S_c and η for natural clays or claystones and compacted bentonite are generally higher
123 than those of the lower plasticity soils.

124 **CORRELATIONS BETWEEN TCF AND SWRC PARAMETERS**

125 The ten soils from the literature listed in Table 1 had data available for calibration of the new
126 TCF and the SWRC of Lu (2016) suitable for the evaluation of quantitative relationships between
127 the TCF and SWRC. Although most of the SWRC datasets were obtained from drying tests or the

128 vapor equilibrium technique, no distinctions are made here for the effects of hydraulic hysteresis,
129 mechanical loading, or volume change along the SWRC that may have occurred in the SWRC
130 measurement. The fitting parameters of the SWRC of Lu (2016) are listed in Table 1.

131 To test the hypothesis of an intrinsic relationship between the SWRC and TCF, a plot of S_c vs.
132 $S_{a,max}$ is shown in Fig. 3(a). Results in the figure show that S_c and $S_{a,max}$ are interrelated, and
133 approximately correspond to the transition from capillarity-dominated to adsorptive dominated
134 water retention mechanisms. The values of S_c and $S_{a,max}$ for lower plasticity soils are smaller, while
135 the values of both parameters for clays are larger. The relationship between S_c and $S_{a,max}$ may be
136 explained by the fact that soils with high adsorption capacity typically contain more clay mineral
137 content and have smaller/flatter soil particles and more micro-size pores. The soil particles can
138 retain more adsorbed water to form water bridges between the neighboring particles leading to
139 higher values of S_c and $S_{a,max}$. The equation relating S_c and $S_{a,max}$ can be expressed as follows:

$$S_c = 0.72 \cdot S_{a,max} + 0.21 \quad (4)$$

140 The coefficient of determination of 0.92 indicates a strong correlation between S_c and $S_{a,max}$.
141 The intercept in Eq. (4) is greater than zero as even soils with low adsorption capacity will have
142 water menisci at particle contacts at the end of capillarity. To further evaluate relationships
143 between the pore size parameters in the TCF and SWRC, the relationship between TCF parameter
144 η in Eq. (3) and SWRC parameter n in Eq. (2) is plotted in Fig. 3(b). A functional relationship
145 between η and n for the different soils can be defined as follows:

$$\eta = 9.92 - 4.39 \cdot n \quad (5)$$

146 The coefficient of determination of Eq. (5) is 0.89 confirms that the pore size distribution plays an
147 important role in both the TCF and SWRC. In summary, the parameter n describes the shape of
148 the SWRC in the capillarity-dominated regimes of the SWRC, while $S_{a,max}$ is the degree of

149 saturation at the transition between capillarity-dominated and adsorption-dominated water
150 retention mechanisms in the SWRC of Lu (2016), which may emphasize that the transition
151 between the water retention mechanisms in the SWRC plays an important role in the shape of the
152 TCF, emphasizing the importance of linking the TCF parameters to those of the SWRC of Lu
153 (2016) as opposed to the more empirical SWRC of van Genuchten (1980).

154 The parameter λ_{dry} in the TCF can be measured or potentially theoretically considered closely
155 related to the soil particle contact form and area. Further, the soil mineralogy and associated
156 microstructure also contribute to the maximum matric suction in the SWRC (Lu and Khorshidi
157 2015). It is hypothesized that the thermal conductivity of dry soil λ_{dry} is related with the maximum
158 matric suction ψ_{max} for a given soil. The correlation between λ_{dry} in the TCF and ψ_{max} in the SWRC
159 shown in Fig. 3(c) follows a linear relationship with a best-fit equation given as follows:

$$\lambda_{\text{dry}} = 4.1 \times 10^{-7} \cdot \psi_{\text{max}} \quad (6)$$

160 A high coefficient of determination of 0.93 indicates that the adsorptive water retention mechanism
161 and soil mineralogy may play a role in the shape of the tail end of the TCF. However, the thermal
162 conductivity in dry conditions is also strongly affected by the dry density in addition to mineralogy.
163 Although the dry density may also affect the maximum suction in soils, this has not been
164 established experimentally. Accordingly, it is recommended to measure the thermal conductivity
165 values for dry and saturated conditions as specialized suction control techniques are not needed.
166 With experimental values of λ_{sat} and λ_{dry} , the correlations for S_c and η in Eqs. (4) and (5) can be
167 used to predict the shape of the TCF from the SWRC.

168 **VALIDATION**

169 The correlations between the parameters of the TCF and SWRC in Figs. 3(a) and 3(b) were
170 used to predict the TCF of a soil that was not included in the database in Table 1. Specifically, the

171 transient evolution in thermal conductivity was measured during constrained hydration of a
172 bentonite layer in a tank-scale test reported by Lu and McCartney (2023). The λ_{dry} and λ_{sat} values
173 were from laboratory measurements, while the parameters S_c and η were predicted by Eqs. (4) and
174 (5) using the SWRC parameters by Lu and McCartney (2022). Further, the measured value of λ_{dry}
175 is close to a calculated value of 0.237 by Eq. (6), with an error of less than 3%, confirming the
176 possible correlations between parameter λ_{dry} and ψ_{max} in Fig. 4. A good fit was observed between
177 the predicted TCF and the experimental data in Fig. 4, which reflects the feasibility of using the
178 correlations established in this study to predict the shape of the TCF from the SWRC. The
179 nonlinear evolution in thermal conductivity observed at the beginning of hydration is attributed to
180 transient local volume changes in the bentonite layer.

181 **CONCLUSIONS**

182 An improved isothermal thermal conductivity function was proposed for fine-grained
183 unsaturated soils and calibration with soils from the literature indicates that the new TCF captures
184 the sigmoidal evolution in the thermal conductivity with changing degree of saturation and has an
185 equal or better fit to experimental data for different fine-grained soils at both low and high
186 saturation regimes compared to existing models. Correlations between the TCF parameters and
187 those of the SWRC of Lu (2016) were established, indicating a relationship between the point of
188 curvature parameter in the TCF and the maximum adsorption saturation, and a relationship
189 between the shape parameter of the TCF and the pore size distribution parameter from the SWRC.
190 The maximum suction from the SWRC was correlated with the thermal conductivity in dry
191 conditions, as both variables are dependent on the soil mineralogy. A validation example from a
192 long-term tank-scale test involving nonisothermal hydration of bentonite confirms that it is

193 possible to estimate the TCF for fine-grained soils from the SWRC parameters along with
194 measurements of the thermal conductivity in dry and saturated conditions.

195 **ACKNOWLEDGEMENTS**

196 The authors appreciate support from U.S. Department of Energy’s Nuclear Energy University
197 Program award DE-NE008951. The views in this paper are those of the authors alone.

198 **DATA AVAILABILITY STATEMENT**

199 All data, models, and code generated or used during the study appear in the submitted article.

200 **REFERENCES**

- 201 Behbehani, F., and J. S. McCartney. 2022. “Energy pile groups for thermal energy storage in
202 unsaturated soils.” *Appl. Therm. Eng.* 215: 119028.
- 203 Cao, T. D., S. K. Thota, F. Vahedifard, and A. Amirlatifi. 2021. “General thermal conductivity
204 function for unsaturated soils considering effects of water content, temperature, and confining
205 pressure.” *J. Geotech. Geoenviron. Eng.* 147 (11): 04021123.
- 206 Cho, W. J., J. O. Lee, and S. Kwon. 2011. “An empirical model for the thermal conductivity of
207 compacted bentonite and a bentonite–sand mixture.” *Heat Mass Transf.* 47 (11): 1385–1393.
- 208 Côté, J., and J. M. Konrad. 2005. “A generalized thermal conductivity model for soils and
209 construction materials.” *Can. Geotech. J.* 42 (2): 443–458.
- 210 Dong, Y., N. Lu, A. Wayllace, and K. Smits. 2014. “Measurement of thermal conductivity function
211 of unsaturated soil using a transient water release and imbibition method.” *Geotech. Test. J.*
212 37 (6): 980–990.
- 213 Dong, Y., J. S. McCartney, and N. Lu. 2015. “Critical review of thermal conductivity models for
214 unsaturated soils.” *Geotech. Geol. Eng.* 33 (2): 207–221.

215 Johansen, O. 1975. "Varmeledningsevne av jordarter (Thermal conductivity of soils)." University
216 of Trondheim, Trondheim. US Army Corps of Engineers, Cold Regions Research and
217 Engineering Laboratory, Hanover, N.H. CRREL Draft English Translation 637.

218 Likos, W. J. 2014. "Modeling thermal conductivity dryout curves from soil-water characteristic
219 curves." *J. Geotech. Geoenviron. Eng.* 140 (5): 04013056.

220 Lu, N. 2016. "Generalized soil water retention equation for adsorption and capillarity." *J. Geotech.*
221 *Geoenviron. Eng.* 142 (10): 04016051.

222 Lu, N., and Y. Dong. 2015. "Closed-form equation for thermal conductivity of unsaturated soils
223 at room temperature." *J. Geotech. Geoenviron. Eng.* 141 (6): 04015016.

224 Lu, N., J. W. Godt, and D. T. Wu. 2010. "A closed-form equation for effective stress in unsaturated
225 soil." *Water Resour. Res.* 46 (5): W05515.

226 Lu, N., and M. Kaya. 2013. "A drying cake method for measuring suction-stress characteristic
227 curve, soil-water-retention curve, and hydraulic conductivity function." *Geotech. Test. J.* 36
228 (1): 1–19.

229 Lu, N., and M. Khorshidi. 2015. "Mechanisms for soil-water retention and hysteresis at high
230 suction range." *J. Geotech. Geoenviron. Eng.* 141 (8): 04015032.

231 Lu, S., T. Ren, Y. Gong., and R. Horton. 2007. "An improved model for predicting soil thermal
232 conductivity from water content at room temperature." *Soil Sci. Soc. Am. J.* 71 (1): 8–14.

233 Lu, Y., and J. S. McCartney. 2022. "Physical modeling of coupled thermohydraulic behavior of
234 compacted MX80 bentonite during heating." *Geotech. Test. J.* 45 (6): 20220054.

235 Lu, Y., and J. S. McCartney. 2023. "Insights into the thermo-hydraulic properties of compacted
236 MX80 bentonite during hydration under elevated temperature." *Can. Geotech. J.*
237 <https://doi.org/10.1139/cgj-2022-0537>.

238 Lu, Y., W. M. Ye, Q. Wang, Y. H. Zhu, Y. G. Chen, and B. Chen. 2020. "Investigation on
239 anisotropic thermal conductivity of compacted GMZ bentonite." *Bull. Eng. Geol. Environ.* 79
240 (3): 1153–1162.

241 Lu, Y., W. M. Ye, Q. Wang, Y. H. Zhu, Y. G. Chen, and B. Chen. 2021. "Anisotropic swelling
242 behaviour of unsaturated compacted GMZ bentonite hydrated under vertical stresses." *Bull.*
243 *Eng. Geol. Environ.* 80 (7): 5515–5526.

244 McCartney, J. S., E. Jensen, and B. Counts. 2013. "Measurement of the impact of volume change
245 on thermal conductivity of subgrade soils." *TRB 2013*. Washington, DC. Jan. 13–17. pp. 1–9.

246 Madsen, F. T. 1998. "Clay mineralogical investigations related to nuclear waste disposal." *Clay*
247 *Miner.* 33 (1): 109–129.

248 McInnes, K. 1981. "*Thermal conductivities of soils from dryland wheat regions in eastern*
249 *Washington*." Ph.D. Dissertation, Washington State University, Pullman, WA.

250 van Genuchten, M. T. 1980. "A closed- form equation for predicting the hydraulic conductivity
251 of unsaturated soils." *Soil Sci. Soc. Am. J.* 44 (5): 892–898.

252 Villar, M. V. 2002. "*Thermo-hydro-mechanical characterisation of a bentonite from Cabo de Gata.*
253 *A study applied to the use of bentonite as sealing material in high level radioactive waste*
254 *repositories*." ENRESA, Madrid.

255 Xiao, Y., H. Liu, B. Nan, and J. S. McCartney. 2018. "Gradation-dependent thermal conductivity
256 of sands." *J. Geotech. Geoenviron. Eng.* 144 (9): 06018010.

257 Xiao, Y., G. Ma, J. S. McCartney, and B. Nan. 2020. "Thermal conductivity of granular soils with
258 contrasting particle shapes." *J. Geotech. Geoenviron. Eng.* 146 (5): 06020004.

259 Xiao, Y., Y. Tang, G. Ma, J. S. McCartney, and J. Chu. 2021. "Thermal conductivity of
260 biocemented graded sands." *J. Geotech. Geoenviron. Eng.* 147 (10): 04021106.

261 Yao, J., T. Wang, and W. J. Likos. 2019 “Measuring thermal conductivity of unsaturated sand
262 under different temperatures and stress levels using a suction-controlled thermo-mechanical
263 method.” *Geo-Congress 2019*, 784–793. Reston, VA: ASCE.

264 Ye, W. M., Y. Lu, X. H. Huang, B. Chen, Y. G. Chen, and Y. J. Cui. 2017. “Anisotropic thermal
265 conductivity of unsaturated compacted GMZ bentonite-sand mixture.” *Proc., 2nd PanAm.*
266 *Conf. Unsat. Soil.*, Dallas, Texas, 413–424.

267 Zheng, L., J. Samper, L. Montenegro, and A. M. Fernández. 2010. “A coupled THMC model of a
268 heating and hydration laboratory experiment in unsaturated compacted FEBEX bentonite.” *J.*
269 *Hydro.* 386 (1–4): 80–94.

270

271 LIST OF FIGURE CAPTIONS

272 **Fig. 1.** TCF calibration for fine-grained soils: (a) Bonny silt; (b) Palouse silt loam; (c) Denver
273 claystone; (d) Georgia kaolinite.

274 **Fig. 2.** TCF calibration for compacted bentonites: (a) GMZ; (b) GMZ; (c) GMZ07; (d) MX80;
275 (e) Kyungju; (f) FEBEX.

276 **Fig. 3.** Relationships between TCF parameters and those of the SWRC of Lu (2016): (a) S_c and
277 $S_{a,max}$; (b) η and n ; (c) Relationship between TCF parameter λ_{dry} and Lu (2016) SWRC
278 parameter ψ_{max} .

279 **Fig. 4.** Validation of transient evolution in thermal conductivity of MX80 bentonite in a tank-
280 scale test by Lu and McCartney (2023).

Table 1. Physical, thermal, and hydraulic properties of ten fine-grained soils

No.	Name and reference	θ_s (m ³ /m ³)	ρ_d (Mg/m ³)	λ_{dry} (W/mK)	λ_{sat} (W/mK)	Parameters of the SWRC of Lu (2016)					
						α (1/kPa)	n (-)	ψ_c (kPa)	$S_{a,max}$ (m ³ /m ³)	m (-)	ψ_{max} (kPa)
1	Bonny silt ^a	0.43	1.50	0.350	1.250	0.058	1.74	3000	0.046	0.13	7.9×10^5
2	Palouse silt loam ^b	0.53	1.25	0.210	0.950	0.080	1.38	60000	0.243	0.40	7.0×10^5
3	Denver claystone ^{c,d}	0.51	1.31	0.410	1.050	0.0040	1.54	20000	0.392	0.15	1.0×10^6
4	Georgia kaolinite ^{c,d}	0.51	1.28	0.239	1.556	0.0100	1.70	20000	0.171	0.01	6.0×10^5
5	GMZ ^e	0.44	1.50	0.580	1.370	0.0009	1.35	45000	0.459	0.22	1.4×10^6
6	GMZ ^f	0.36	1.70	0.600	1.420	0.0002	1.32	60000	0.550	0.22	1.4×10^6
7	GMZ07 ^g	0.42	1.60	0.362	1.220	0.0002	1.55	30000	0.562	0.15	9.0×10^5
8	MX80 ^h	0.41	1.60	0.340	0.935	0.0003	1.45	30000	0.571	0.16	7.0×10^5
9	Kyungju ⁱ	0.40	1.60	0.350	1.220	0.0005	1.24	40000	0.552	0.25	9.0×10^5
10	FEBEX ^j	0.43	1.53	0.480	1.050	0.0002	1.45	50000	0.495	0.25	1.2×10^6

282 ^aDong et al. (2014); ^bMcInnes (1981); ^cLu and Kaya (2013); ^dLu and Dong (2015); ^eLu et al. (2020); ^fYe et al. (2017);

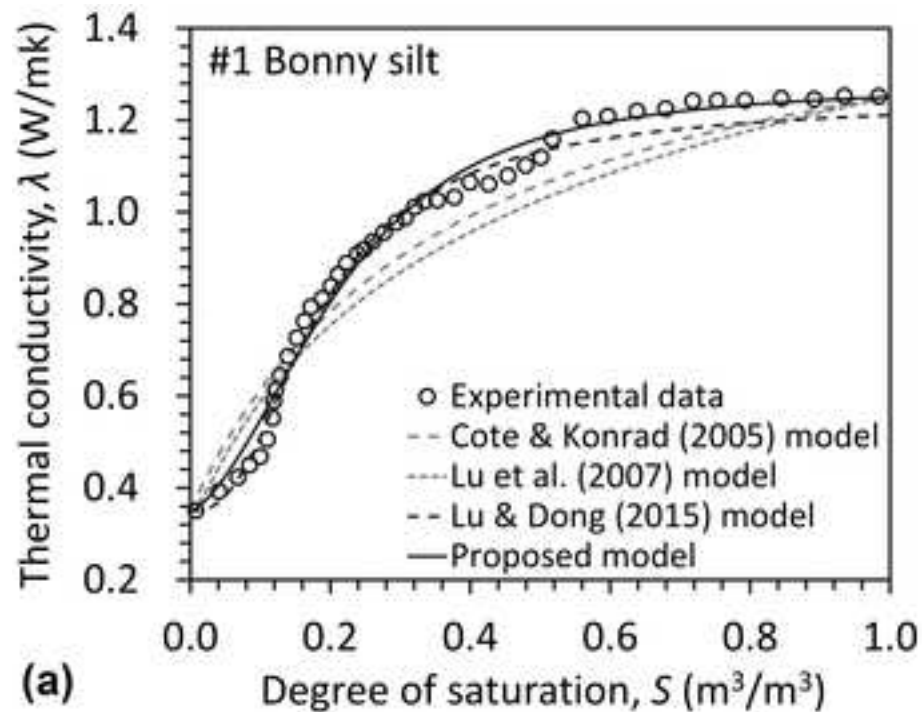
283 ^gXu et al. (2019); ^hMadsen (1998); ⁱCho et al. (2011); ^jVillar (2002).

284

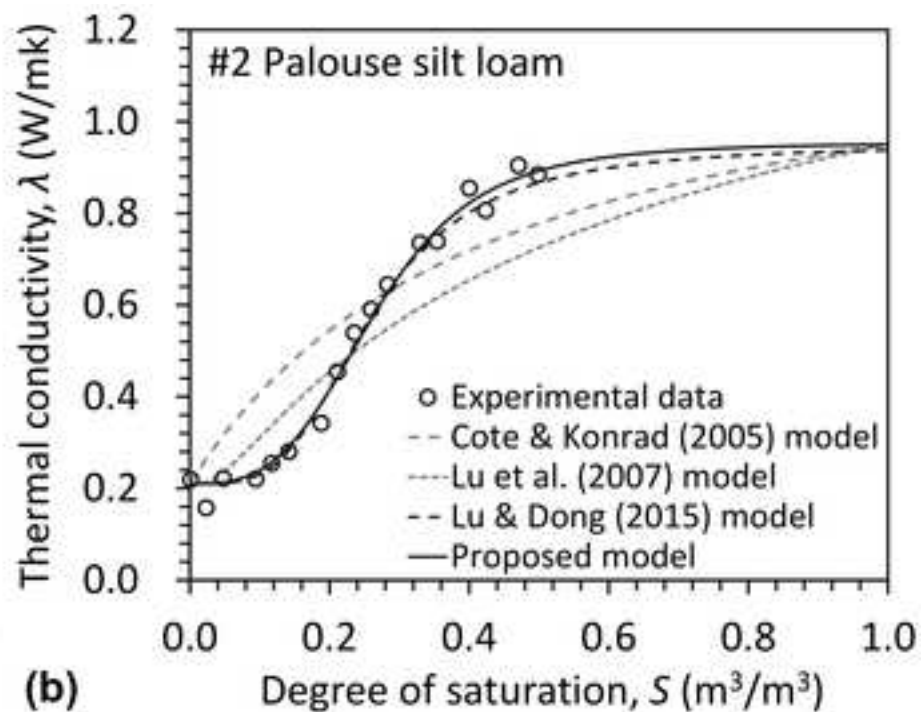
285 **Table 2.** Fitting parameters for the newly proposed TCF and other TCFs from the literature (Bold: Model
286 with best fit; Underlined: Soils where new model has the second best fit)

Soil	Côté & Konrad (2005)			Lu et al. (2007)			Lu & Dong (2015)				Proposed TCF			
	κ	R^2	$RMSE$	β	R^2	$RMSE$	S_r	γ	R^2	$RMSE$	S_c	η	R^2	$RMSE$
Bonny silt	3.72	0.893	0.074	0.95	0.850	0.090	0.145	2.62	0.985	0.033	0.283	2.44	0.985	0.033
Palouse silt loam	3.30	0.546	0.117	0.78	0.596	0.111	0.233	3.81	0.988	0.027	0.295	3.96	0.990	0.026
Denver claystone	2.10	0.902	0.049	0.28	0.988	0.021	0.217	2.63	0.979	0.026	0.405	2.76	<u>0.981</u>	0.027
Georgia kaolinite	3.18	0.900	0.105	0.92	0.897	0.109	0.171	2.92	0.992	0.036	0.280	2.80	0.998	0.018
GMZ	0.96	0.839	0.078	0.53	0.567	0.110	0.432	4.75	0.983	0.032	0.540	4.07	0.998	0.012
GMZ	0.90	0.688	0.064	0.54	0.104	0.133	0.468	4.63	0.983	0.020	0.580	4.31	0.989	0.018
GMZ07	1.15	0.965	0.051	0.52	0.926	0.079	0.363	3.50	0.968	0.054	0.629	2.87	0.995	0.022
MX80	0.98	0.994	0.017	0.55	0.913	0.066	0.442	4.20	0.950	0.052	0.600	3.30	<u>0.976</u>	0.037
Kyungju	0.78	0.882	0.062	0.57	-0.029	0.161	0.546	5.95	0.924	0.062	0.640	4.60	0.969	0.039
FEBEX	0.75	0.994	0.013	0.59	0.976	0.035	0.440	3.51	0.997	0.010	0.610	3.51	0.998	0.009

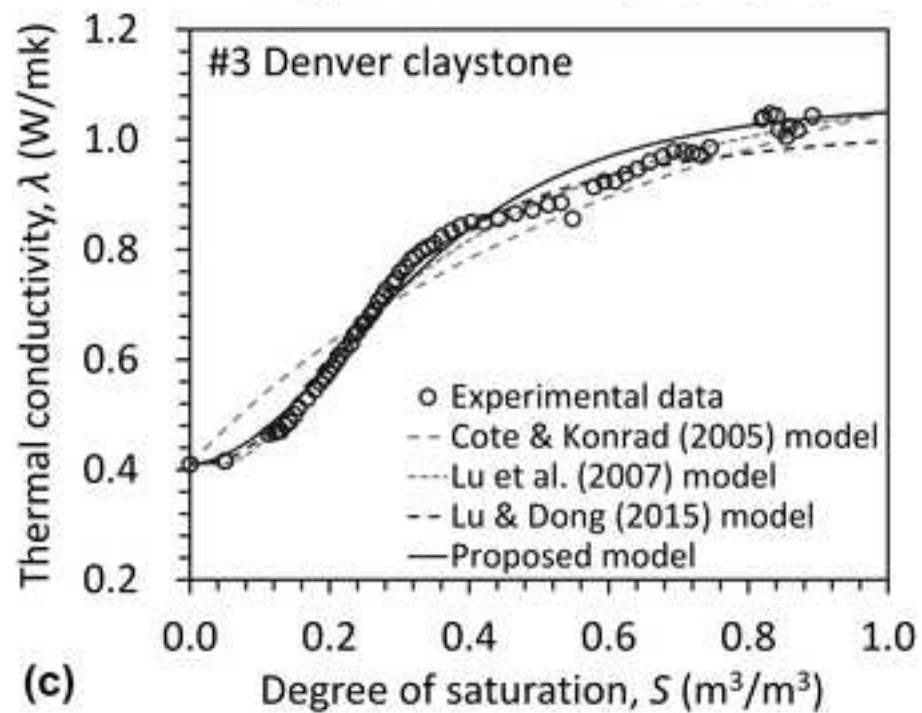
287



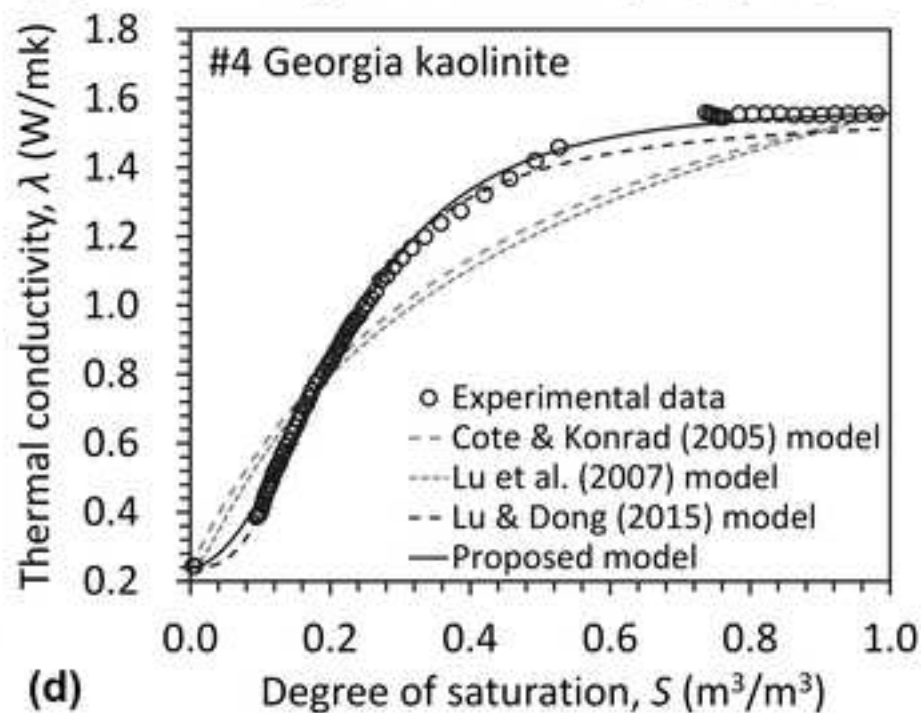
(a)



(b)



(c)



(d)

